Accepted Manuscript

The alkaline transition of cytochrome *c* revisited: Effects of electrostatic interactions and tyrosine nitration on the reaction dynamics

Santiago Oviedo-Rouco, María A. Castro, Damián Alvarez-Paggi, Cecilia Spedalieri, Verónica Tortora, Florencia Tomasina, Rafael Radi, Daniel H. Murgida

PII: S0003-9861(19)30071-2

DOI: https://doi.org/10.1016/j.abb.2019.02.016

Reference: YABBI 7961

To appear in: *Archives of Biochemistry and Biophysics*

Received Date: 29 January 2019

Revised Date: 18 February 2019

Accepted Date: 19 February 2019

Please cite this article as: S. Oviedo-Rouco, Marí.A. Castro, Damiá. Alvarez-Paggi, C. Spedalieri, Veró. Tortora, F. Tomasina, R. Radi, D.H. Murgida, The alkaline transition of cytochrome *c* revisited: Effects of electrostatic interactions and tyrosine nitration on the reaction dynamics, *Archives of Biochemistry and Biophysics* (2019), doi: https://doi.org/10.1016/j.abb.2019.02.016.

The Alkaline Transition of Cytochrome *c* Revisited: Effects of Electrostatic Interactions and Tyrosine Nitration on the Reaction Dynamics

*Santiago Oviedo-Rouco,[†] María A. Castro,[†] Damián Alvarez-Paggi,[†§] Cecilia Spedalieri,[†] Verónica Tortora,[‡] Florencia Tomasina,[‡] Rafael Radi,[‡] and Daniel H. Murgida[†]**

[†]Departamento de Química Inorgánica, Analítica y Química Física and INQUIMAE (CONICET-UBA), Facultad de Ciencias Exactas y Naturales, Universidad de Buenos Aires, Ciudad Universitaria, Pab. 2, piso 1, Buenos Aires C1428EHA, Argentina

[‡]Departamento de Bioquímica and Center for Free Radical and Biomedical Research, Facultad de Medicina, Universidad de la Republica, Av. Gral. Flores 2125, Montevideo 11800, Uruguay

*Corresponding Author: E-mail: dhmurgida@qi.fcen.uba.ar Phone.: +54-11-5285-8208

ORCID Daniel H. Murgida: 0000-0001-5173-0183

[§]Present Address INFANT Foundation, Buenos Aires, Argentina.

ABSTRACT

Here we investigated the effect of electrostatic interactions and of protein tyrosine nitration of mammalian cytochrome *c* on the dynamics of the so-called alkaline transition, a pH- and redox-triggered conformational change that implies replacement of the axial ligand Met80 by a Lys residue. Using a combination of electrochemical, time-resolved SERR spectroelectrochemical experiments and molecular dynamics simulations we showed that in all cases the reaction can be described in terms of a two steps minimal reaction mechanism consisting of deprotonation of a triggering group followed by ligand exchange. The pK_a^{alk} values of the transition are strongly modulated by these perturbations, with a drastic downshift upon nitration and an important upshift upon establishing electrostatic interactions with a negatively charged model surface. The value of pK_a^{alk} is determined by the interplay between the acidity of a triggering group and the kinetic constants for the forward and backward ligand exchange processes. Nitration of Tyr74 results in a change of the triggering group from Lys73 in WT Cyt to Tyr74 in the nitrated protein, which dominates the pK_a^{alk} downshift towards physiological values. Electrostatic interactions, on the other hand, result in strong acceleration of the backward ligand exchange reaction, which dominates the pK_a^{alk} upshift. The different physicochemical conditions found here to influence pK_a^{alk} are expected to vary depending on cellular conditions and subcellular localization of the protein, thus determining the existence of alternative conformations of Cyt *in vivo*.

Keywords: cytochrome *c*, alkaline transition, time-resolved SERR, protein nitration, protein spectroelectrochemistry, protein electron transfer

1. INTRODUCTION

Mitochondrial cytochrome *c* (Cyt) is a c.a. 13 kDa globular protein that contains a single heme covalently attached through the two cysteine residues of a conserved Cys-Xaa-Xaa-Cys-His binding motif, where the His residue (His18 in horse heart Cyt) is axially coordinated to the heme iron. The coordination sphere is completed by a Met residue (Met80 in horse heart Cyt) at the sixth axial position.[1,2] This Met/His axial coordination pattern corresponds to the so-called native conformation or state III, which prevails for wild type (WT) Cyt at physiological pH and in the absence of perturbations. The axial coordination pattern and other structural and dynamic features endow native Cyt with optimized thermodynamic and kinetic parameters for performing its canonical function at the intermembrane mitochondrial space, i.e. shuttling electrons between complexes III and IV in the respiratory electron transfer (ET) chain.[3] On the other hand, it is now accepted that Cyt behaves as a moonlighting protein, meaning that the actual structure and function vary depending on intracellular localization, specific and unspecific interactions and post-translational chemical modifications.[4] For example, in the intermembrane space Cyt behaves as an electron shuttle in healthy cells, but gains peroxidase activity upon interaction with negatively charged cardiolipin under pro-apoptotic conditions.[5] Liberation of Cyt to the cytosol seals the fate of the cell through formation of the apoptosome complex, a crucial component of the cell suicide machinery.[6] Cyt may also penetrate the nucleus and prevent nucleosome assembly.[7] Moreover, a number of naturally occurring mutations and post-translational modifications[8–11] have been described to affect the structure and function of Cyt to some extent, although in most cases the details remain largely unknown. The cornerstone of Cyt multifunctionality is believed to be its high flexibility, which enables the exploration of a broad conformational space. This feature allows populating a variety of conformations, depending of

the specific conditions, that may differ in axial coordination pattern, redox parameters, binding affinities, catalytic activity, etc.[4,12–14]

The native structure of horse Cyt consists of five α-helical and two short β-sheet elements interconnected by Ω loops of different lengths.[15–17] Alternative conformations of Cyt may be attained by different means such as pH variation, electrostatic interactions with phospholipids and other negatively charged model systems or interactions with cytochrome *c* oxidase. A feature in common among these nonnative species is the loss of the axial ligand Met80 in ferric Cyt without significantly affecting the α-helical content.[3,18,19] Instead, distortions are mostly localized at the level of the Ω loop 70-85, which contains the labile Met80 ligand, as well as in the Ω loop 40-57.[18,20] Note that these two loops also constitute the first two foldons that are thermally disrupted in the uphill denaturation pathway model developed by Englander and coworkers.[14,21] Both loops are interconnected via a H-bonding network that contains Tyr67 as a prominent member that, thereby, shapes the dynamical features relevant to both the canonical ET reaction as well as to alternative functions of Cyt. Interestingly, the 70-85 loop not only contains the axial ligand that is removed upon interaction with model and real partners, but it also includes most of the Lys residues that surround the partially exposed heme edge, which constitute the positively charged patch involved in electrostatic interactions with negatively charged counterparts.[22,23] Thus, the flexible 70-85 loop and its response to local electric fields,[24] specific electrostatic interactions,[25,26] chemical modifications[27,28] and other perturbations appear to be critical for the different functions of Cyt.

In this context, the so-called alkaline transition represents a window of opportunity for accessing the dynamics of conformational changes of Cyt that involve the Ω loop 70-85 through controlled physicochemical experiments.

The alkaline transition of ferric Cyt is a pH-dependent conformational change that was first identified by Theorel and Åkenson almost 80 years ago.[29] Latter studies demonstrated that the process implies the loss of the axial ligand Met80, which is replaced by a Lys residue to yield a Lys/His axial coordination pattern.[30] Mutational analysis has demonstrated that the sixth axial position in the Lys/His isomer of horse Cyt is occupied by either Lys73 or Lys79,[31,32] i.e. two residues belonging to the critical Ω loop 70-85. Thus, the alkaline form Lys/His, also known as state IV, is actually a mixture of two species with chemically equivalent axial coordination pattern. The 3D structure of the alkaline conformation of WT Cyt remains elusive, although the structures of double and triple mutants of yeast Cyt that feature a Lys73 sixth axial ligand have been resolved by NMR and X-ray crystallography, constituting good structural models of state IV.[33,34] These models confirm a globular structure very similar to the WT protein at neutral pH, with the most important deviations localized in the 70-85 loop region.

For horse Cyt the Met/His ⇄ Lys/His equilibrium is characterized by pK_a^{alk} = 9.4, and this value differs only slightly for cytochromes from other species.[35] Due to this unphysiologically high pK_a^{alk}, the alkaline transition has long been considered a model for studying related conformational changes of Cyt that also involve the 70-85 loop, but not biologically relevant per se.[14] This perspective has changed in recent years with the discovery that oxidative post-translational modifications[27] as well as naturally occurring and artificial single mutations, such as Gly41Ser and Tyr48Glu, respectively, induce “early alkaline transitions” at nearly neutral

pH.[8,36] So far three pathogenic naturally occurring single point mutations of human Cyt have been identified, and 16 others, which are awaiting further characterization, have been found by massive sequencing of exomes.[3,37] Moreover, it is now well established that Cyt may undergo different post-translational modifications, such as phosphorylation,[8] sulfoxidation,[9] methylation,[38] acetylation[39] and nitration.[10] Among them, nitration of Tyr74, which occurs under oxidative stress conditions, results in pK_a^{alk} values very close to the physiological pH.[11,27,28] Based on a model system, a similar pK_a^{alk} downshift has been predicted for the phosphorylation of Tyr48.[8]

The mechanism of the alkaline transition for WT Cyt has been extensively studied employing a variety of kinetic experimental techniques and was found to be very complex and has not yet been completely elucidated.[13,14,20,21,30,32,40] Combination of stopped-flow and NMR-based hydrogen exchange experiments reveal that the main kinetic features can be rationalized in terms of a minimal two steps mechanism.[21] The first step is the deprotonation of a triggering group, and is followed by a rate limiting structural change of the Ω loop 70-85, which leads to the replacement of Met80 by either Lys73 or Lys79 previously deprotonated (Scheme 1).[21]

Scheme 1. Minimal reaction mechanism for the alkaline transition of ferric Cyt

$$Cyt^{3+} - H_{state\ III} \overset{K_H}{\rightleftarrows} Cyt^{3+}_{state\ III} \underset{k_b}{\overset{k_f}{\rightleftarrows}} Cyt^{3+}_{state\ IV}$$

Although extensively discussed, the nature of the triggering group that is deprotonated in the first step of Scheme 1 remains unknown. Based on the acidity estimated for this group in WT

Cyt, pK_H = 11, the surface exposed Lys residues are likely candidates, but other possibilities cannot be excluded.

Interestingly, the slow phase represented in Scheme 1 coincides with the minimal mechanism originally proposed by Davis et. al.,[40] and the parameters of these two coupled equilibria quantitatively explain the apparent pK_a^{alk} of the alkaline transition experimentally determined through stationary acid-base titration (equation 1), thus providing good basis for further dynamical studies of this pH-dependent ligand exchange reaction:

$$pK_a^{alk} = pK_H + log\frac{k_b}{k_f} \qquad (1)$$

Note that all the above mentioned mechanistic studies refer to the WT protein and selected artificial point mutants, but not to naturally occurring mutations or post-translational modifications that are known to shift the apparent pK_a^{alk} towards physiological values. Moreover, all the kinetic studies reported so far were performed with diluted protein solutions, thereby excluding some important features of the in vivo environment that may affect the process. One of these aspects is the fact that more than 15% of the mitochondrial Cyt is not free in the intermembrane space but associated to membrane components such as the negatively charged binding domains of complexes II and IV and to the negatively charged lipid cardiolipin.[3,41,42] Thus, a large fraction of Cyt is, at least temporarily, under the action of high local electric fields and specific electrostatic interactions that preferentially involve the Lys residues belonging to the crucial Ω loop 70-85.

In the present work we address the effect of electrostatic interactions on the dynamics and thermodynamics of the alkaline transition for WT Cyt and a variant nitrated at Tyr74 (NO_2-Cyt), which is a post-translational modification that has been demonstrated to occur in vivo under

oxidative stress conditions[10] and to produce a drastic downshift of pK_a^{alk}.[27,28] The experimental strategy adopted for this investigation is the use of electrodes coated with self-assembled monolayers (SAMs) of carboxyl-terminated alkanethiols as artificial electrostatic partners of the investigated proteins. These simplified model systems are clearly unable to mimic a number of dynamical and structural aspects of the lipidic and protein components of the mitochondrial membrane, but are still useful to capture some essential features of the electrostatic interactions of Cyt.[43–45]

Most notably, adsorption of Cyt to SAM-coated electrodes implicates the same set of positively charged residues that constitute the binding domain towards natural electrostatic partners such as Cyt oxidase, Cyt reductase, Cyt peroxidase and cardiolipin.[22,23,46] A specific advantage of the electrode-SAM/Cyt model systems that we exploit in the present work is that the adsorbed protein undergoes efficient direct electrochemistry, thus enabling the possibility of triggering the alkaline transition through an oxidative potential jump, and the subsequent monitoring of the conformational transition through time-resolved surface-enhanced resonance Raman (TR-SERR) spectroelectrochemistry.[43,47] A somewhat related concept of conformationally gated homogeneous electron transfer has been introduced by Bowler and coworkers to study the pH-dependent Met/His ligand exchange reaction of non-native yeast iso-Cyt variants using stopped-flow methodology.[48,49]

The results presented here demonstrate that electrostatic interactions and post-translational modifications of Cyt may tune pK_a^{alk} through modulation of the thermodynamic and kinetic parameters of the proposed two steps minimal reaction mechanism.

2. MATERIALS AND METHODS

2.1. Materials. Horse heart cytochrome *c* (Cyt; BioUltra, ≥99%), buffer CHES, 11-mercapto-1-undecanol and 11-mercapto-1-undecanoic acid were purchased from Merck and used without further purification. Cyt nitrated at Tyr74 (NO_2-Cyt) and the triple mutants H33N/H26N/Y67F and H33N/H26N/Y74F (hereafter Tyr67Phe and Tyr74Phe, respectively) were produced as previously described.[27,28] All experiments were conducted with type II water (R > 18 MΩ) purified in a Milli-Q system.

2.2. Cyclic voltammetry. Electrochemical experiments were performed with a Gamry REF600 potentiostat using a thermostatized cell at 25°C placed into a Faraday cage (Vista Shield) equipped with a polycrystalline gold bead working electrode, a Pt wire auxiliary electrode and a Ag/AgCl (3.5 M KCl) reference electrode. Au electrodes were treated with a 3:1 v/v H_2O_2:H_2SO_4 mixture at 120 °C. The electrodes were then subjected to repetitive voltammetric cycles between −0.2 and 1.6 V in 10% $HClO_4$ and thoroughly washed with water and ethanol. Afterwards, Au electrodes were coated with self-assembled monolayers (SAMs) by overnight incubation into a 1 mM:1 mM ethanolic solution of a HS-$(CH_2)_6$-CH_2OH : HS-$(CH_2)_6$-COOH mixture. The SAM-coated electrodes were incubated for ca. 4 hrs into a 400 μM protein solution, then rinsed and inserted into the electrochemical cell. All electrochemical determinations were performed in CHES/sulfate buffer 12.5:12.5 mM.

2.3. Raman spectroelectrochemistry. Stationary and time-resolved surface-enhanced resonance Raman experiments were performed using a three-electrode spectroelectrochemical cell mounted in front of a confocal microscope coupled to a single-stage spectrograph (Dilor XY; f = 800 mm) equipped with a 1800 lines/mm grating and a liquid nitrogen-cooled back-illuminated CCD detector (2048 × 512 pixels) at room temeperature, ca. 25°C. Different laser

lines were employed for spectral acquisition depending on the specific experiments: 406 nm (~3.5mW; solid state laser TopMode-HP-406), 458 nm (~8 mW; argon ion laser Coherent Innova 70c) or 514 nm (13 mW, argon ion laser Coherent Innova 70c). The silver ring working electrodes were mechanically polished and subjected to oxidation-reduction cycles in 0.1 M KCl to create SERR-active nanostructured surfaces. Subsequently, the Ag rings were incubated in 2 mM ethanolic solutions of the alkanethiols (1:1 mixture of HS-$(CH_2)_{10}$-CH_2OH and HS-$(CH_2)_{10}$-COOH) for ca. 24 h and transferred to the spectroelectrochemical cell. The SAM-coated silver ring was mounted on a shaft that is rotated at about 5 Hz to avoid laser-induced sample degradation. The electrode potential was controlled with a TeQ03 potentiostat. The spectroelectrochemical cell typically contained 8 mL of 0.2 μM protein solution at the desired pH. Spectral accumulation times were between 10 and 30 s. Before each experiment, the spectrometer was calibrated employing Hg and Na calibration lamps and controlled using silicon and 4-acetamidophenol. The spectrometer parameters were set to obtain a 0.4 cm^{-1} increment per data point.

For TR-SERR experiments, potential jumps from -300 mV to 210 mV and variable duration were applied to trigger the reaction. The SERR spectra were measured at different delay times following the potential jump. Synchronization of potential jumps and probe laser pulses was achieved by a pulse-delay generator (BNC). The probe pulses were generated by passing the cw laser beam through two consecutive laser intensity modulators (QIOPTICS Photonics), which give a total extinction better than 1:50000 and a time response of ca.20 ns.

After background subtraction, the SERR spectra were subjected to component analysis as originally described by Döpner et. al.[50] In this method, the experimental spectra are fitted using complete spectra of the different species involved, which are determined independently.

The only adjustable parameters are the relative contributions of the different component spectra, while the spectral parameters of each component (positions, widths, and relative intensities of the different bands) are kept constant. After subtracting the spectral contributions of residual redox inactive fractions, concentrations profiles were fitted to the set of differential equations that describe the reaction mechanism shown in Scheme 3 using a self-written routine.

2.4. Computational methods. The starting structure for molecular dynamics (MD) simulations of Cyt in the ferric state corresponds to the oxidized form of WT horse heart Cyt (PDB ID 1HRC). All simulations were performed both in presence and absence of crystallographic water molecules and no significant differences were observed. The PMEMD module of the AMBER16 package[51] with the ff99 force field implementation was used for every MD calculation. All structures were minimized in a TIP3P water box and an initial MD at constant volume was performed to heat the system to 300 K. Then, a constant pressure simulation was performed to equilibrate the system density.

Production simulations were performed for 50 ns at 300 K and 1 bar and were maintained with the Berendsen thermostat and barostat respectively.[52] Periodic boundary conditions and Ewald sums were used for treating long-range electrostatic interactions. The SHAKE algorithm was used to keep bonds involving H atoms at their equilibrium length.[53]

NO_2-Cyt was built in silico by replacing the corresponding side chains and relaxing the resulting structure using classical MD. Partial charges for the protonated and deprotonated nitro-tyrosine were obtained from RESP calculations computed using Hartree–Fock with a 6-31G basis set.[54] Finally, production runs of 50 ns were obtained for WT Cyt, NO_2-Cyt, deprotonated NO_2-Cyt and WT Cyt with deprotonated Lys73.

Hydrogen bonds (H-bonds) were considered when the donor(D)-acceptor(A) distance was less than 3.0 Å and the D-H-A angle was less than 20°.

Constant pH simulations were performed with the CpHMD method[55] in order to compute pK_a values. This method performs a periodic Monte Carlo (MC) sampling of protonation states along a standard generalized Born implicit solvent simulation. At each MC step, a titratable site and a new protonation state for that site are randomly chosen and the transition free energy is computed. This energy is then used as the basis for applying the Metropolis criterion[56] to determine whether the transition will be accepted or not. This value depends on both the environment of the titrated residue and the solvent pH. If the transition is accepted, the MD simulation continues with the titrable residue in the new protonation state. Otherwise, the MD continues with no changes in the protonation state. In this work, several calculations were performed for every system in order to evaluate the consistency of the results as titrable residues may influence each other. One calculation was performed including all possible titrable residues, other calculation was done with a subset of relevant titrable residues (Lys 72, Lys 73, Lys 79, Glu 66, Tyr 67, Tyr 74). Finally, calculations including only one titrable residue were performed for each residue of the subset. NO_2-Tyr74 was not included as titrable residue as it was not implemented in the method.

The pKa value for each residue was then computed based on the population of the protonated and deprotonated states using Henderson-Hasselbach's equation.

3. RESULTS AND DISCUSSION

3.1 The alkaline transition of Cyt in electrostatic complexes. As a simple model system for assessing the effect of electrostatic interactions on the alkaline transition of Cyt, we employed metal electrodes coated with SAMs obtained from 1:1 mixtures of 11-mercapto-1-undecanol and

11-mercapto-1-undecanoic acid. Cyt electrostatically adsorbed on these SAM-coated electrodes display quasi-reversible CV response at pH 7.0, with the characteristic features of a surface-confined one electron redox couple and a midpoint potential of 190 mV (Figure 1). This number represents a relatively small downshift with respect to the value determined for the protein in solution under identical pH and ionic strength conditions, which is ascribed to the interfacial potential drop across the SAM, as well as to differences in the adsorption constants of ferric and ferrous Cyt, as previously established by different groups.[57,58]

The SERR spectrum of the adsorbed protein recorded at open circuit, pH 7.0 and under Soret-band excitation is identical to the RR spectrum of ferric Cyt in solution measured under otherwise identical conditions, thus confirming the structural integrity of the adsorbed protein at the level of the heme pocket. Increasing the pH to 11.5, i.e. well above the value of pK_a^{alk} in solution, induces a number of small but significant and reproducible changes in the high and low frequency regions of the SERR spectrum (Figure 2). The skeletal modes that appear in the high frequency region are particularly sensitive to the porphyrin core size and electron density and, therefore, constitute characteristic markers of the oxidation and spin states.[18,19,43] The small upshifts observed for these bands are consistent with the pH-induced formation of an alternative six-coordinated high spin species, most likely as the result of the replacement of Met80 with another strong-field distal ligand such as His or Lys to yield either Lys/His or His/His axial coordination patterns.[18,19,26,43] The low frequency spectral region allows for a clear distinction between these two possible axial coordination motifs of the heme iron. As shown in Figure 2, the SERR spectrum recorded at pH 11.5 differs from reference spectra previously reported for the Met/His and His/His species and, instead, are almost identical to the RR spectra obtained for Cyt in solutions of pH 10.5 and 11.5. These results constitute strong evidence that

ferric Cyt presents the same axial coordination at pH 11.5 in solution and in the adsorbed state, and that this species can be safely assigned to the Lys/His alkaline conformer.

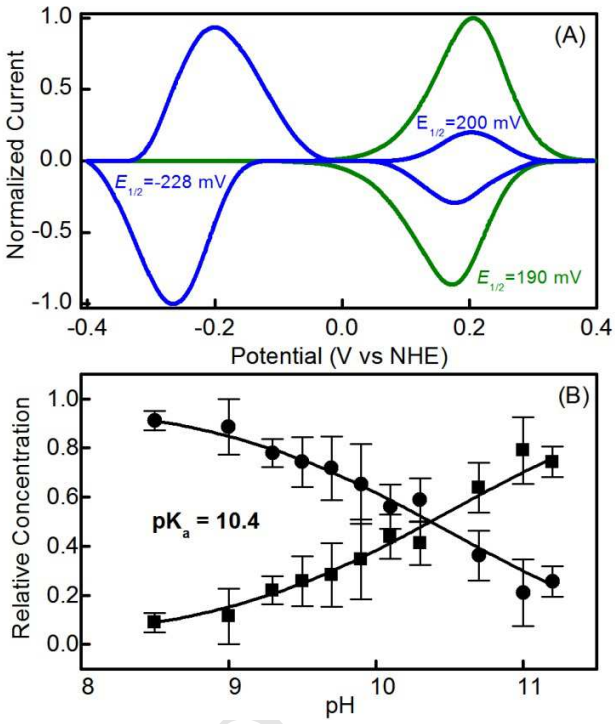

Figure 1. (A) Background corrected normalized cyclic voltammetries of WT Cyt adsorbed on a SAM-coated electrode recorded a 10 V s^{-1}. Green and blue traces were acquired at pH 7.0 and 11.5, respectively. Unprocessed data are shown in Figure S1. (B) Relative surface concentrations of the native and alkaline conformations of WT Cyt estimated from the relative areas of the CV peaks for both redox couples acquired at 10 Vs^{-1} as a function of pH.

In contrast to the results obtained at neutral pH, the CV responses recorded at alkaline pH display two well defined redox couples at high scan rates, which become increasingly irreversible at lower scan rates, thus indicating a relatively slow redox-coupled conformational equilibrium between the two electroactive species (Figures 1 and S2). The first redox couple is assigned to the native Met/His Cyt conformation as the midpoint potential is very similar to the

value obtained in neutral solution and is only slightly pH-dependent, in agreement with previous observations.[58] For the second redox couple the midpoint potential is -228 mV, i.e. very similar to the value previously reported for alkaline Cyt in solution[59] and, therefore, is assigned to the Lys/His isomer.

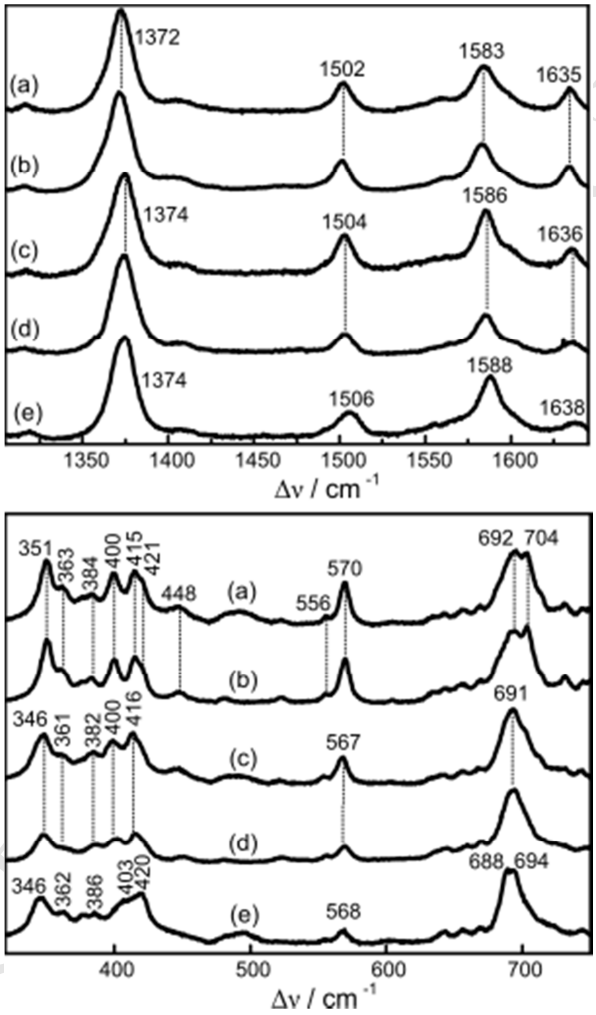

Figure 2. High frequency (upper panel) and low frequency (lower panel) resonance Raman and surface-enhanced resonance Raman spectra of ferric WT Cyt obtained with Soret-band excitation under different experimental conditions: (a) in solution at pH 7.0, (b) adsorbed at pH 7.0 and open circuit, (c) in solution at pH 10.5, (d) adsorbed at pH 11.0 and open circuit, (e) in solution at pH 7.0 with added cardiolipin liposomes, taken from reference [26].

Taken together, the CV and SERR data indicate a redox-coupled conformational equilibrium between the native and alkaline conformations of adsorbed Cyt, with the Met/His and Lys/His conformers having essentially the same heme pocket structure as the corresponding species in solution.

The pK_a^{alk} of adsorbed Cyt was estimated from the relative intensities of voltammetric waves obtained for both redox couples at high scan rates as a function of pH. As shown in Figure 1, the speciation diagram obtained in this way yields pK_a^{alk} = 10.4, which is one pH unit higher than the corresponding value in solution.[28] Independent SERR titrations confirm this result. In these latter experiments SERR spectra of adsorbed Cyt are measured as a function of the solution pH at an applied potential of 310 mV. The measured high frequency spectra are subjected to component analysis using SERR reference spectra recorded at pH 7.0 and 11.5 for extracting the pure native and alkaline components, respectively (Figure S3). SERR titrations were performed up to pH values around 11.5, which implies ca. 70 % conversion to the alkaline conformation, as more alkaline conditions induce protein desorption. These experiments yield pK_a^{alk} = 10.0 (Figure S4) that, within experimental error, is very similar to the value determined by CV. The upshift of pK_a^{alk} for adsorbed Cyt compared to the protein in solution may be related to an upshift of the pK_H of the triggering group (Scheme 1) or to changes in the kinetics of ligand exchange, as will be discussed in the next section.

Stationary potential-dependent SERR measurements of immobilized Cyt at pH 10.2, i.e. very close to the determined pK_a^{alk}, reveal that both the native and alkaline ferric Cyt forms respond to the applied electrode potential. In this case, however, the apparent reduction potentials obtained

from the speciation diagrams (Figure 3) are not true potentials as this analysis is based on steady state concentrations of coupled reactions. Most importantly, the spectral analysis reveals the presence of a single ferrous component that corresponds to the Met/His native conformation, thus indicating that the reduction of the alkaline form is coupled to a Lys/His→Met/His transition that is completed within the time window of the steady-state experiments. In contrast to the results obtained at neutral pH, the SERR experiments performed at pH 10.2 reveal that a minor fraction of the adsorbed protein, ca. 10%, remains in the Met/His oxidized form even at very negative potentials, which probably indicates the existence at this pH of a subpopulation of the adsorbed protein that is not properly oriented for establishing efficient direct electrochemistry.

Stationary SERR measurements performed under Q-band excitation at a constant applied electrode potential of 350 mV show that for the Met/His spectral component of adsorbed ferric Cyt the intensity ratio of the bands ν_{10} and ν_4 at 1633 and 1371 cm^{-1}, respectively, decreases upon increasing the pH (Figure S5). As previously shown,[60] the ν_{10} band corresponds to an A_{1g} mode that is expected to undergo preferential SERR enhancement when the heme plane is parallel to the surface, while B_{1g} modes such as the ν_4 band are preferentially enhanced for a perpendicularly oriented heme. Therefore, the $I(\nu_{10})/I(\nu_4)$ intensity ratio is a measure of the average orientation of the adsorbed Cyt.[60] The observed decrease of $I(\nu_{10})/I(\nu_4)$ with pH indicates a less perpendicular average orientation of the adsorbed Cyt in increasingly alkaline media, as also predicted by molecular dynamics simulations,[22,61] which is consistent with a small fraction of electrochemically inactive Cyt. Neglecting the fraction of redox inactive Cyt, which can be accurately determined and subtracted for further quantitative analysis, the

electrochemical and spectroelectrochemical results can be summarized in terms of the square reaction model presented in Scheme 2.

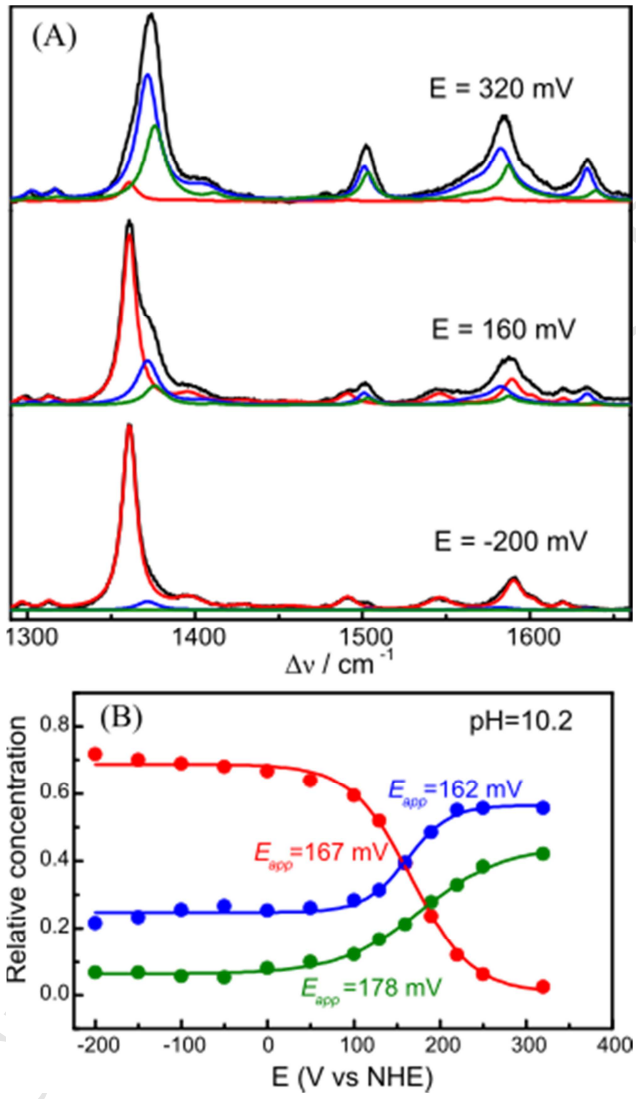

Figure 3. (A) SERR spectra of WT Cyt adsorbed on a SAM-coated electrode, as a function of the electrode potential. Black traces are the experimentally measured spectra, while color lines are the spectral components that correspond to native ferrous Cyt (red), native ferric Cyt (blue) and alkaline ferric Cyt (green). All the spectra were recorded with Soret-band excitation at pH 10.2. (B) Relative surface concentrations of the different Cyt forms obtained by SERR as a function of the applied potential. The color code is the same used in the upper panel.

The midpoint potentials of both redox couples in this scheme, as well as pK_a^{alk} for the ferric protein, are experimentally accessible, while pK_a^{alk} for ferrous Cyt can be derived from the other three quantities, yielding a value of 17. This result is consistent with the fact that stationary SERR spectra measured at sufficiently negative potentials reveal a single ferrous spectral component that corresponds to the native Met/His conformation, and with the fact that a quasireversible CV response of the alkaline conformer is only observed at very high scan rates.

Scheme 2. Coupled redox and conformational equilibria of WT Cyt and NO_2-Cyt adsorbed on SAM-coated electrodes. The parameters indicated in blue and green correspond to WT Cyt and NO_2-Cyt, respectively.

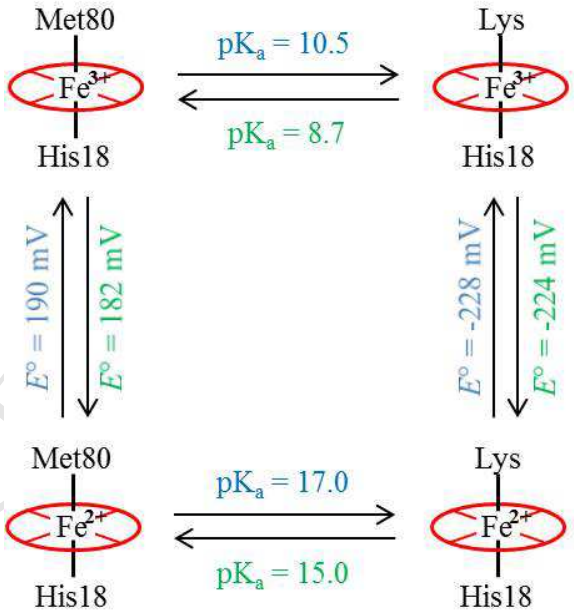

Similar experiments were performed for Cyt nitrated at Tyr74 (NO_2-Cyt) adsorbed on SAM-coated electrodes. The adsorbed NO_2-Cyt exhibits a quasireversible CV response at pH 7.0 with a midpoint potential of 182 mV, i.e. very similar to native Met/His conformation of WT Cyt

(Figure S6). Voltammograms recorded at pH 10 and high scan rates also show a single quasireversible redox couple, but with a midpoint potential of -224 mV that is assigned to the Lys/His alkaline conformation. SERR spectra recorded under identical conditions confirm the assignment of the two redox couples to the Met/His and Lys/His conformations at neutral and alkaline pH, respectively (Figure S7). These results suggest that for the adsorbed NO_2-Cyt pK_a^{alk} is upshifted with respect to the value of 7.1 previously determined for the same protein variant in solution.[27,28] Indeed, acid-base titrations of the adsorbed protein monitored by SERR (Figure S8) yield pK_a^{alk} = 8.7 for the ferric protein. These results suggest that Scheme 2 also applies to NO_2-Cyt, yielding pK_a^{alk} = 15 for the ferrous form.

3.2. Kinetic studies of the alkaline transition. The results presented in the preceding section and summarized in Scheme 2 set the basis for investigating the dynamics of the alkaline transition in electrostatic Cyt/SAM complexes taking advantage of the seven orders of magnitude difference in the K_a^{alk} values of ferric and ferrous Cyt. These findings imply that, both for WT Cyt and NO_2-Cyt, the equilibrium concentration of the ferrous Lys/His isomer is negligible small at any pH and applied potential and, therefore, Scheme 2 can be cast in a simplified form:

Scheme 3. Simplified redox-coupled conformational equilibrium of WT Cyt and NO_2-Cyt adsorbed on SAM-coated electrodes.

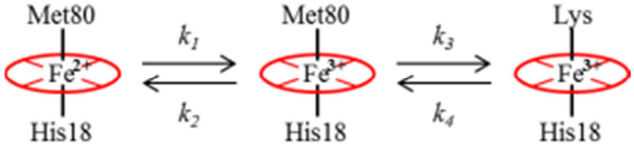

The simplified reaction Scheme 3 highlights the fact that the alkaline transition can be triggered by rapid oxidation of ferrous Cyt at fixed pH, as an alternative to the traditional pH-jump experiments based on stopped-flow technology. With this idea in mind, we investigated the redox-coupled conformational transitions of WT Cyt and NO_2-Cyt adsorbed on SAM-coated electrodes by synchronizing triggering potential jumps applied to the working electrode with time-resolved SERR (TR-SERR) spectral monitoring of the adsorbed species.[43] Specifically, working electrodes were equilibrated at an initial potential of -300 mV to ensure full reduction of the adsorbed protein. The redox-coupled conformational transitions were triggered by applying square potential jumps of sufficient duration to a final potential of 210 mV, i.e above the midpoint potential of the native Cyt conformation. TR-SERR spectra were measured at variable delay times with respect to the start point of the square potential pulse (Figure S9). After each potential jump the system was allowed to equilibrate at the initial potential for a sufficiently long time to ensure recovery of the fresh sample condition, and the entire sequence was repeated until obtaining TR-SERR spectra with acceptable signal-to-noise ratio. As shown in Figures 4 and S10, the TR-SERR spectra could be consistently simulated employing only the same three spectral components found in the stationary experiments, which correspond to the species included in Scheme 3, both for the WT and the nitrated protein. Representative concentration profiles obtained with this methodology for WT Cyt and NO_2-Cyt are shown in Figure 5.

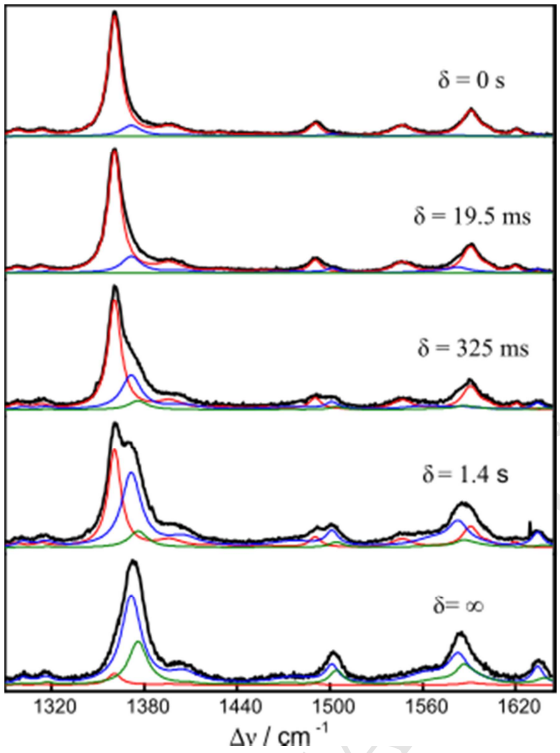

Figure 4. Time-resolved SERR spectra obtained for WT Cyt adsorbed on a SAM coated electrode as a function of the delay time (δ) after applying a potential jump from E_i = -300 mV to E_f = 210 mV. Black: experimental data. Red: ferrous native Cyt spectral component. Blue: ferric native Cyt spectral component. Green: ferric alkaline Cyt spectral component. Experiments were performed at pH 10 with Soret-band excitation.

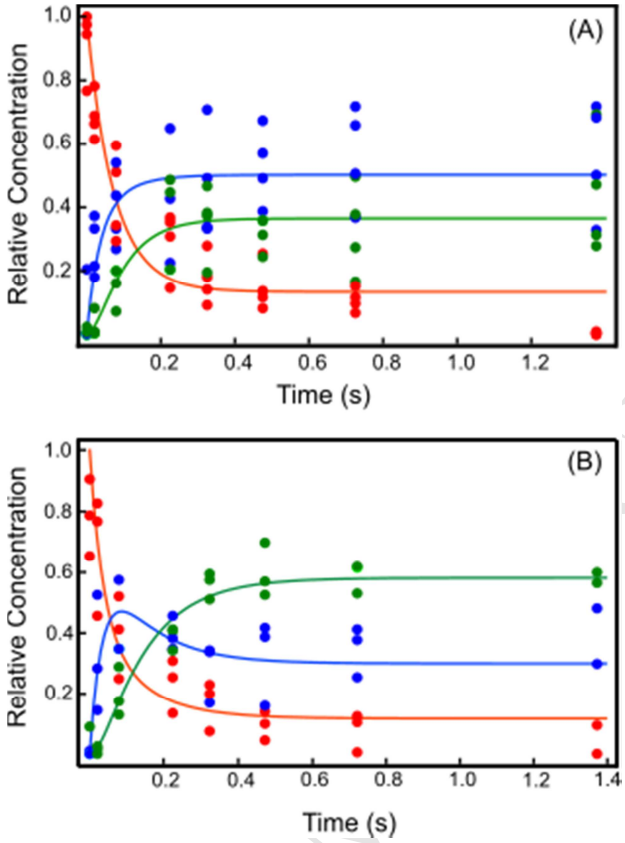

Figure 5. Relative surface concentrations as a function of time of native ferrous (red) native ferric (blue) and alkaline ferric (green) components obtained by TR-SERR for WT Cyt (A) and NO_2-Cyt (B) adsorbed on SAM-coated electrodes. Experiments were performed at pH 10.0 with Soret-band excitation. The lines are best fittings to the reaction scheme 3.

A prerequisite for obtaining reliable kinetic information from this experimental approach is that the triggering redox reaction should not be rate limiting. Compliance of this requirement was controlled for each data set by evaluating the time evolution of the concentration ratios of native oxidized versus alkaline oxidized species, which should not be constant at short delay times. Concentration profiles obtained from 3 to 6 independent experiments that fulfill this condition were then fitted to the kinetic model represented in scheme 3 assuming first order in every

species, to determine the rate constants k_1, k_2, k_3 and k_4. Representative fittings obtained for WT Cyt and NO_2-Cyt are shown in Figure 5. Note that the species assigned in these spectroelectrochemical experiments as native ferric Cyt actually correspond to the sum of the species denoted as $Cyt^{3+} - H_{state\ III}$ and $Cyt^{3+}_{state\ III}$ in Scheme 1 because the protonated and deprotonated forms are spectroscopically indistinguishable and, therefore, rate constants in Schemes 1 and 3 are related as follows:

$$k_3 = K_H k_f / (K_H + [H^+]) \qquad (2)$$

$$k_4 = k_b \qquad (3)$$

According to equation 2, k_3 values were determined by TR-SERR as a function of pH to extract K_H and k_f (Figure 6). For WT Cyt the experiments were limited to the pH range 9.6-10.5, as the alkaline conformation is not detectable at pH < pK_a^{alk}-1 and, on the other hand, pH > 10.5 leads to significant protein desorption. Within this pH range k_3 does not show the expected sigmoidal variation with pH, thus indicating that pK_H > 10.5 for WT Cyt. In contrast, the lower pK_a^{alk} of NO_2-Cyt allows expanding the pH window down to 7.5 and, thereby, the observation of a clear sigmoidal dependence for this protein variant. Linearization of these data allows extracting K_H and k_f from plots $(k_3\text{-}k_0)^{-1}$ *vs* $[H^+]$ (Figure S11), where k_0 is an empirical parameter that accounts for some offset in the k_3 values, which may arise either from systematic errors or from a subpopulation of the adsorbed protein with pH-independent kinetics. The kinetic parameters obtained in this way are summarized in Table 1. Note that, as a strong indication of self-consistency, pK_a^{alk} values experimentally determined by acid-base titration employing stationary SERR detection are nearly identical to those obtained from the kinetic analysis using equation 1 for both protein variants.

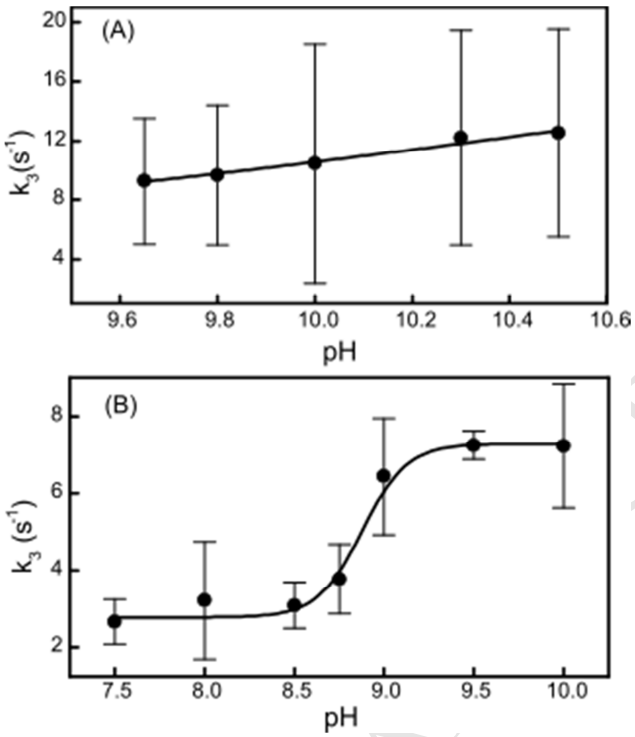

Figure 6. Variation of k_3 with pH as obtained by TR-SERR for WT Cyt (A) and NO_2-Cyt (B) adsorbed on SAM-coated electrodes.

Table 1. Parameters of the alkaline transition for WT Cyt and NO_2-Cyt at 25°C.

	[a]WT Cyt (solution)	[b]WT Cyt (adsorbed)	[b]NO_2-Cyt (adsorbed)
k_f / s^{-1}	6.1±1.8	11±4	5 ± 1
k_b / s^{-1}	0.049	15±4	4±3
k_0 / s^{-1}	-	≈ 8	2.5±0.3
pK_H	11±0.15	10.7±0.3	8.8±0,1
[c] $pK_a^{alk\ calc}$	8.9±2.3	10.8±0.6	8.7±0,5
[d] $pK_a^{alk\ exp}$	9±0.05	10.4±0.1	8.9±0,3

[a]From reference [40]. [b]This work. [c]Calculated using equation 1. [d]From steady state titrations.

Interestingly, while the pK_a^{alk} of WT Cyt is significantly higher in the electrostatic complex compared to the free protein in solution, the acid-base equilibrium of the triggering group is insensitive to adsorption, as K_H values obtained in both conditions are almost identical within experimental error. Thus, the difference in pK_a^{alk} can be quantitatively ascribed to the effect of the electrostatic interactions on the dynamics of the ligand exchange step. This result is not unexpected since the interaction of Cyt with negatively charged counterparts, including natural partner proteins, model membranes and SAMs, involve electrostatic interactions through the ring of positively charged lysine residues in the surface of Cyt that surround the partially exposed

heme edge, and that includes the putative sixth ligands in the alkaline conformation Lys73/79.[22,61] Notably, the electrostatic adsorption does not slow down the ligand exchange reactions as one might anticipate but, in contrast, results in a 2-fold increase of k_f and a much more significant 300-fold increase of k_b, that lead to a 10-fold increase of K_a^{alk}. In an attempt to rationalize the experimental rise of both k_f and k_b, one can describe the ligand exchange step in terms of a reaction coordinate that connects the Met/His and Lys/His conformations via a pentacoordinated activated complex, as previously proposed.[28] Within this model, and assuming that the energy of the activated complex is largely insensitive to adsorption, the experimentally obtained results might reflect the alkaline conformation being destabilized by the specific electrostatic interactions and local electric fields to a greater extent than the native Cyt conformation. Consistent with this hypothesis, previous experimental and computational studies show that the energy and structure of the native conformation is only slightly affected under the current experimental conditions[25,43] and, furthermore, the pentacoordinated species is less destabilized than the Met/His hexacoordinated form.[28]

Adsorption of NO_2-Cyt also results in an upshift of the pK_a^{alk} with respect to the same protein in solution, but the underlying basis for this effect appear to be somewhat different than for WT Cyt. Upon adsorption both protein variants show an increase of k_b with respect to WT Cyt in solution, but the incremental factor for NO_2-Cyt is only 80. In contrast, k_f values measured for both proteins are essentially identical WT within experimental error These results suggest that the alkaline conformation of NO_2-Cyt is significantly less destabilized by electrostatic interactions than the same coordination state of the WT protein. This effect, which tends to increase the pK_a^{alk} value, is overcompensated by a significantly more acidic triggering group with $pK_H = 8.8$.

3.3 On the nature and functioning of the triggering group. The stationary and kinetic results presented above show that the minimal reaction mechanism originally proposed for the alkaline transition of WT Cyt free in solution also applies when the protein is forming an electrostatic complex with a negatively charged SAM. The electrostatic interactions, however, can shift the pK_a^{alk} of the transition either through modulation of the relative stabilities of the Met/His and Lys/His conformers, or by affecting the acidity of the triggering group. Moreover, these variables may be affected by post-translational modifications of Cyt, such as nitration of Tyr residues. The identity of the triggering group, however, remains a matter of debate as comprehensively discussed by Bowler and coworkers.[13,20,48,49] The experimentally determined pK_H of about 11 for WT Cyt both in solution and adsorbed on SAMs argues in favor of a solvent exposed Lys residue in agreement with previous proposals,[13,21,31,40,62] most likely one of the three located in the 70-85 loop, i.e. residues 72, 73 or 79. Based on similar arguments, the solvent exposed Tyr74 residue is another likely candidate. Other proposals include a buried heme propionate,[63] a crystallographic water molecule,[64] the proximal ligand of the heme iron His18,[30] the buried Tyr67,[65] and deprotonation within a hydrogen bonded unit that links Ω-loops 40-57and 71-85.[66] Unequivocal identification of the triggering group has proven rather elusive, but some of these possibilities can be pondered at the light of new experimental and computational evidence. Thus, aiming to assess the possible involvement of Tyr residues as triggers, we generated and titrated the Tyr74Phe and Tyr67Phe mutants. For the Tyr74Phe variant the pK_a^{alk} values obtained for the protein free in solution and adsorbed are 8.9 and 9.9, respectively, i.e. only slightly lower than for WT Cyt under, otherwise, identical conditions (Figure S12). Thus, in agreement with a previous proposal,[27] Tyr74 is unlikely to be the triggering amino acid in the alkaline transition of WT Cyt, even though nitration of this

residue produces a drastic change in the experimentally determined pK_a^{alk} and pK_H values. In contrast, pK_a^{alk} values determined for the Tyr67Phe mutant in solution[27] and adsorbed are 11.0 and 10.2 (Figure S13), respectively. This upshift, however, does not necessarily imply the involvement of Tyr67 as triggering group and, instead, may simply reflect the key role that this residue plays in modulating the protein structure and dynamics.[67] Thus, to get a deeper insight, we estimated the the pK_a of all titrable amino acids of WT Cyt by means of molecular dynamics simulations, as described in the experimental section. These calculations yield pK_a = 12.5 and pK_a > 14, for the solvent exposed Tyr74 and the buried Tyr67, respectively (Figures S14). Both values are significantly higher than the experimentally determined pK_H, thus making very unlikely the involvement of these Tyr residues as triggering groups. On the other hand, MD simulations yield pK_a = 10.6 for Lys73 and 10.0 both for Lys72 and Lys79 (Figure S15). Thus, all the solvent exposed Lys residues belonging to the 70-85 loop have pK_a values very close to the pK_a of free Lys in solution and to the pK_H of WT Cyt, thereby, constituting likely candidates to act as triggering group, with Lys73 showing the best match. A close inspection of the effect of Lys deprotonation on the extended H-bonding network of Cyt provides some additional arguments to select the most likely triggering group. Thus, we performed 50 ns long MD simulations of WT Cyt with all Lys residues protonated and repeated the simulations with one of the three residues of loop 70-85 deprotonated (dp-Lys72, dp-Lys73 and dp-Lys79, respectively). To quantify the effect of deprotonation, we determined the fraction of time along the simulations that individual H-bonds in the Ω loops 40-57 and 70-85 remain formed, according to the criteria defined in the experimental section. The results are summarized in Table S1. The calculations indicate that protonated Lys72 is only H-bonded to Asn70 during a small fraction of time. Aside from interrupting the Lys72-Asn70 H-bond, deprotonation of Lys72 has a significant weakening

effect on the Lys73-Asn70, Lys73-Glu66 and Lys39-Gln42 interactions. Deprotonation of Lys79 disrupts the Lys79-Thr47 and weakens the Lys39-Gln42 interactions, but affects only slightly other H-bonds from the network. Protonated Lys73, in contrast, is engaged in four lasting H-bonding interactions, two of them with Asn70 and the other two with Glu66 and Glu69. Deprotonation of Lys73 results in complete disruption of these four interactions and of the H-bond Tyr48-Ala43, as well as significant weakening of H-bonds Lys39-Gln42, Gln42-Lys53 and Lys72-Asn70, in addition to other more subtle alterations of the H-bonding network. Thus, while the acid-base equilibria of all three Lys residues from loop 70-85 exert some impact on the structural details of loops 40-57 and 70-85, deprotonation of Lys73 appears to trigger the largest rearrangement of both loops (Figure S16), including complete disruption or substantial weakening of the H-bonding interactions of the two possible distal ligands of the alkaline conformation, i.e. Lys73 and Lys79, as a possible prerequisite for the subsequent ligand exchange step.

Nitration of Tyr74 results in a significant downshift of both pK_a^{alk} and pK_H for the alkaline transition of NO_2-Cyt with respect to WT Cyt (Table 1), therefore we titrated the nitrated Tyr74 residue (NO_2-Tyr74) in NO_2-Cyt/SAM complexes by stationary SERR employing 458 nm laser excitation to selectively enhance the vibrational spectrum of the deprotonated NO_2-Tyr74 residue. The results shown in Figure S17 yield $pK_a^{NO2\text{-}Tyr74} = 8.3$, which is 1.2 units above the value previously determined for the same protein in solution.[28] The proximity of the pK_H and $pK_a^{NO2\text{-}Tyr74}$ values determined for the NO_2-Cyt/SAM complexes suggest a change of triggering group from Lys73 in WT Cyt to Tyr74 in NO_2-Cyt. The pK_a values for the remaining titrable residues of NO_2-Cyt were estimated by MD simulations, both for the protonated and deprotonated forms of the NO_2-Tyr74 residue (p-NO_2-Cyt and dp-NO_2-Cyt, respectively). The

calculations predict that for Glu66, an acidic residue that is in close proximity to Tyr74, the pK_a in the dp-NO_2-Cyt form is upshifted by 1 unit with respect to WT-Cyt (Figure S19), thus indicating that the computational method is capable of assessing the effect of electrostatic charges on neighboring amino acids. However, none of the residues that, due to their intrinsic pK_a values in solution are likely candidates to perform as triggering group, exhibits significant changes upon nitration of Tyr74. For example, the pK_a values of lysines 72, 73 and 79 shift less than 0.3 units when comparing their values in WT Cyt, p-NO_2-Cyt and dp-NO_2-Cyt. These results are consistent with NO_2-Tyr74 acting as the triggering group. Interestingly, MD simulations predict that nitration of Tyr74 exerts qualitatively the same effect on the H-bonding network of loops 40-57 and 70-85 as deprotonation of Lys73 in WT Cyt, and this disruption effect is further enhanced upon deprotonation of the NO_2-Tyr74 residue (Table S1 and Figure S18). The most significant changes refer to H-bonds that involve Lys73 as the donor. As schematically shown in Figure 7, in the fully protonated WT protein the pairs of residues Lys73-Glu66 and Lys73-Glu69 remain at H-bonding distance 16% and 26 % of the simulation time, respectively, while 7 % of the time Lys73 is H-bonded to both residues simultaneously, thus the number of H-bonds of Lys73 varies between 0 and 2 along the MD simulation. Either deprotonation of Lys73 or nitration plus deprotonation of Tyr74 affect the time evolution of the H-bonds of residue 73 in very similar fashion. Specifically, the p-NO_2-Cyt and dp-NO_2-Cyt forms, both containing protonated Lys73, show almost complete disruption of the Lys73-Glu66 H-bond and a significantly reduced persistence of the Lys73-Glu69 H-bond (Figure 7 and Table S1). Deprotonation of the NO_2-Tyr residue, in turn, is associated to a further weakening of the Lys73-Glu69 H-bond. Note that nitration of Tyr74 has no significant effect on the H-bonding of Lys79 (Table S1).

Based on these data we propose that the triggering deprotonation event in the alkaline transition mechanism disrupts the hydrogen bond network that involves the two Ω-loops, in agreement with a recent finding by Deacon and coworkers.[66] More specifically, the present data point out the disruption of the Glu66-Lys73-Glu69 H-bonding network as a crucial step for the subsequent Met/Lys ligand exchange that may involve either Lys73 or Lys79. For the WT protein the evidence points out Lys73 as the most likely triggering group, while for the nitrated protein the results are consistent with a qualitatively similar two steps minimal mechanism, except that in this case the reaction is triggered by the early deprotonation of the NO_2-Tyr74 residue.

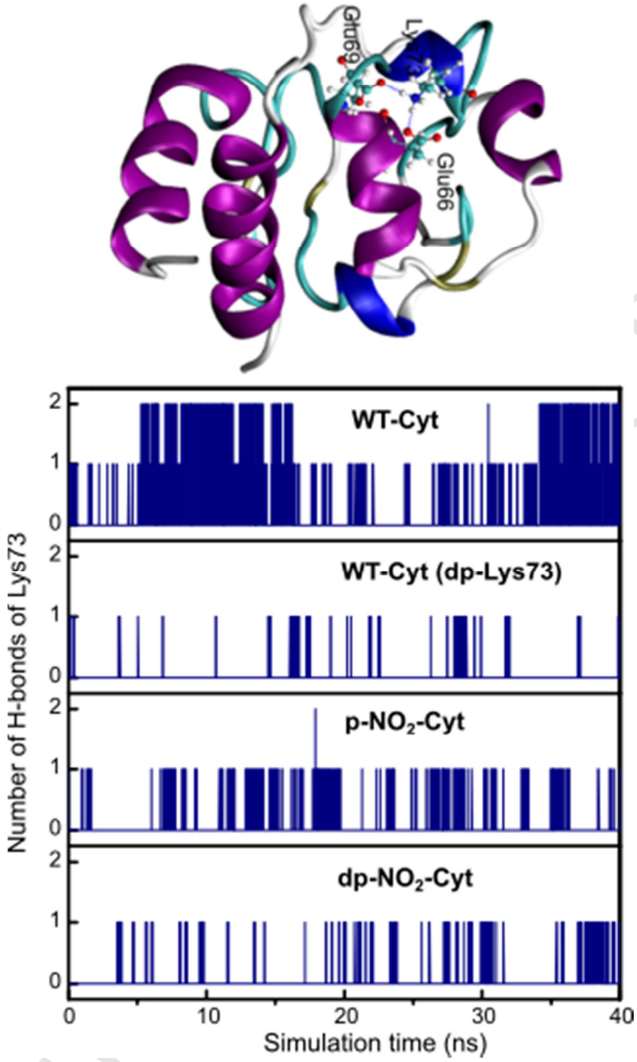

Figure 7. Upper panel: selected snapshot of the MD simulation of WT Cyt displaying a detail of the Glu66-Lys73-Glu69 H-bonds. Lower panel: number of H-bond contacts of Lys73 established along MD simulations for WT Cyt with protonated Lys73 (WT-Cyt), WT cyt with deprotonated Lys73 (dp-Lys73) and the nitrated forms p-NO_2-Cyt and dp-NO_2-Cyt, both with residue Lys73 in the protonated state.

4. CONCLUSIONS

Electrostatic adsorption of WT Cyt and NO_2-Cyt onto a negatively charged model surface results in a similar downshift of the apparent redox potential of both proteins with respect to

solution that is not paralleled by changes in the heme pocket structure and, therefore is ascribed to: (i) differences in the binding constants of the ferric versus ferrous proteins and (ii) to the potential drop across the complex electrode/SAM/protein/bulk interface. In their ferric states, both proteins adsorbed on SAM-coated electrodes undergo alkaline transitions that, according to the kinetic studies reported here, follow a mechanism qualitatively similar to WT Cyt in solution. The equilibrium constant for this conformational equilibrium in the reduced state is negligibly small (10^{-15}-10^{-17}), which explains that the reduced form of the Lys/His isomer cannot be detected in stationary experiments.

Based on spectroelectrochemical studies and MD simulations, we assign Lys73 as the most likely triggering group for the alkaline transition of WT Cyt. Similar studies reveal a change of triggering group from Lys73 to Tyr74 in NO_2-Cyt, which results in an early alkaline transition with pK_a^{alk} = 7.1, i.e. within the range of the physiological pH of the mitochondrial intermembrane space.[68] The pK_a^{alk} values of both protein variants are upshifted by about 1-1.6 units with respect to solution when adsorbed on SAM-coated electrodes. In contrast, the pK_H of the triggering group of WT Cyt is not affected by adsorption. This contrasting behavior of pK_a^{alk} and pK_H suggests that the differences between adsorbed and dissolved proteins cannot be rationalized in terms of a locally different pH at the interface with respect to the bulk solution. Instead, the pK_a^{alk} value reflects the interplay between the thermodynamic K_H parameter and the dynamics of the ligand exchange step expressed through the rate constants k_f and k_b. The TR-SERR experiments reveal that k_f is largely insensitive to adsorption. In contrast, k_b increases more than two orders of magnitude for the immobilized proteins with respect to WT Cyt in solution. These results can be rationalized in terms of preferential electrostatic destabilization of

the alkaline conformer compared to the native conformation and the pentacoordinated activated complex.

Thus, in summary, post-translational nitration of Cyt results in an early alkaline transition at physiological pH which, therefore, might be of biological significance, probably related to an increase of peroxidatic activity as previously observed.[27,28] Electrostatic interactions of WT Cyt and NO_2-Cyt with a model SAM-coated substrate have the effect of preventing the alkaline transition at physiologically relevant pH due to the upshift of the pK_a^{alk} by more than 1 unit. Blockage of the alkaline transition at physiological pH as a consequence of electrostatic interactions is a result that one might anticipate on the basis that adsorption to SAM-coated electrodes involves the Lys residues belonging to the Ω-loop 70-85, which then might lose degrees of freedom required for undergoing the ligand exchange reaction. The present results reveal the counterintuitive fact that the Met/His→Lys/His is not slowed down upon adsorption via the loop 70-85. Instead, the upshift of the pKa in the adsorbed state is explained by a drastic acceleration of the back ligand exchange reaction Lys/His→Met/His.

Certainly, the SAM/Cyt electrostatic complexes are simplified model systems that are unable to capture the specific interactions and mobility of real electrostatic partners of Cyt and, therefore, conclusions extracted in the present work cannot be directly extrapolated to in vivo conditions. However, the physicochemical concept that perturbations such as post-translational chemical modifications and electrostatic interactions may modulate pK_a^{alk} in either direction through the relative magnitudes of K_H, k_f and k_b appears to be general, thereby anticipating the possibility of Cyt attaining alternative conformations in vivo, depending on the specific cellular conditions and subcellular localization.

SUPLEMENTARY DATA

Supplementary data to this article can be found online at…

NOTES

The authors declare no competing interest

ACKNOWLEDGMENT

This work was supported by ANPCyT, Argentina (PICT2015-0133), University of Buenos Aires, Argentina (UBACYT20020170100141BA), Universidad de la República, Uruguay (CSIC Grupos 2014 and Espacio Interdisciplinario Centros 2015),ANII, Uruguay (FCE-1-2014-1-104233). SOR is a doctoral CONICET fellow. FT was partially supported by a fellowship from Universidad de la República and additional support from PEDECIBA. MAC, DAP and DHM are CONICET staff members.

REFERENCES

[1] I. Bertini, G. Cavallaro, A. Rosato, Cytochrome *c* : Occurrence and Functions, Chem. Rev. 106 (2006) 90–115. doi:10.1021/cr050241v.

[2] Scott, R.A., ed., Cytochrome c: A Multidisciplinary Approach, Sausalito, CA, 1996.

[3] D. Alvarez-Paggi, L. Hannibal, M.A. Castro, S. Oviedo-Rouco, V. Demicheli, V. Tórtora, F. Tomasina, R. Radi, D.H. Murgida, Multifunctional Cytochrome c: Learning New Tricks from an Old Dog, Chem. Rev. 117 (2017) 13382–13460. doi:10.1021/acs.chemrev.7b00257.

[4] L. Hannibal, F. Tomasina, D.A. Capdevila, V. Demicheli, V. Tórtora, D. Alvarez-Paggi, R. Jemmerson, D.H. Murgida, R. Radi, Alternative Conformations of Cytochrome c: Structure, Function, and Detection, Biochemistry. 55 (2016) 407–428. doi:10.1021/acs.biochem.5b01385.

[5] V.E. Kagan, V.A. Tyurin, J. Jiang, Y.Y. Tyurina, V.B. Ritov, A.A. Amoscato, A.N. Osipov, N.A. Belikova, A.A. Kapralov, V. Kini, I.I. Vlasova, Q. Zhao, M. Zou, P. Di, D.A. Svistunenko, I.V. Kurnikov, G.G. Borisenko, Cytochrome *c* acts as a cardiolipin oxygenase required for release of proapoptotic factors, Nat. Chem. Biol. 1 (2005) 223–232. doi:10.1038/nchembio727.

[6] S. Yuan, C.W. Akey, Apoptosome Structure, Assembly, and Procaspase Activation, Structure. 21 (2013) 501–515. doi:10.1016/j.str.2013.02.024.

[7] K. González-Arzola, I. Díaz-Moreno, A. Cano-González, A. Díaz-Quintana, A. Velázquez-Campoy, B. Moreno-Beltrán, A. López-Rivas, M.A.D. la Rosa, Structural basis for inhibition of the histone chaperone activity of SET/TAF-Iβ by cytochrome c, Proc. Natl. Acad. Sci. 112 (2015) 9908–9913. doi:10.1073/pnas.1508040112.

[8] J.M. García-Heredia, A. Díaz-Quintana, M. Salzano, M. Orzáez, E. Pérez-Payá, M. Teixeira, M.A. De la Rosa, I. Díaz-Moreno, Tyrosine phosphorylation turns alkaline transition into a biologically relevant process and makes human cytochrome c behave as an anti-apoptotic switch, J. Biol. Inorg. Chem. 16 (2011) 1155–1168. doi:10.1007/s00775-011-0804-9.

[9] D.A. Capdevila, W.A. Marmisollé, F. Tomasina, V. Demicheli, M. Portela, R. Radi, D.H. Murgida, Specific methionine oxidation of cytochrome c in complexes with zwitterionic lipids by hydrogen peroxide: Potential implications for apoptosis, Chem. Sci. 6 (2015) 705–713. doi:10.1039/c4sc02181a.

[10] R. Radi, Protein Tyrosine Nitration: Biochemical Mechanisms and Structural Basis of Functional Effects, Acc. Chem. Res. 46 (2013) 550–559. doi:10.1021/ar300234c.

[11] J.M. García-Heredia, I. Díaz-Moreno, P.M. Nieto, M. Orzáez, S. Kocanis, M. Teixeira, E. Pérez-Payá, A. Díaz-Quintana, M.A. De la Rosa, Nitration of tyrosine 74 prevents human cytochrome c to play a key role in apoptosis signaling by blocking caspase-9 activation, Biochim. Biophys. Acta BBA - Bioenerg. 1797 (2010) 981–993. doi:10.1016/j.bbabio.2010.03.009.

[12] P. Weinkam, J. Zimmermann, F.E. Romesberg, P.G. Wolynes, The Folding Energy Landscape and Free Energy Excitations of Cytochrome c, Acc. Chem. Res. 43 (2010) 652–660. doi:10.1021/ar9002703.

[13] M.M. Cherney, B.E. Bowler, Protein dynamics and function: Making new strides with an old warhorse, the alkaline conformational transition of cytochrome c, Coord. Chem. Rev. 255 (2011) 664–677. doi:10.1016/j.ccr.2010.09.014.

[14] H. Maity, J.N. Rumbley, S.W. Englander, Functional role of a protein foldon—An Ω-loop foldon controls the alkaline transition in ferricytochrome c, Proteins Struct. Funct. Bioinforma. 63 (2006) 349–355. doi:10.1002/prot.20757.

[15] G.W. Bushnell, G.V. Louie, G.D. Brayer, High-resolution three-dimensional structure of horse heart cytochrome c, J. Mol. Biol. 214 (1990) 585–595. doi:10.1016/0022-2836(90)90200-6.

[16] L. Banci, I. Bertini, J.G. Huber, G.A. Spyroulias, P. Turano, Solution structure of reduced horse heart cytochrome c, JBIC J. Biol. Inorg. Chem. 4 (1999) 21–31. doi:10.1007/s007750050285.

[17] L. Banci, I. Bertini, H.B. Gray, C. Luchinat, T. Reddig, A. Rosato, P. Turano, Solution Structure of Oxidized Horse Heart Cytochrome c, Biochemistry. 36 (1997) 9867–9877. doi:10.1021/bi970724w.

[18] S. Oellerich, H. Wackerbarth, P. Hildebrandt, Spectroscopic Characterization of Nonnative Conformational States of Cytochrome c, J. Phys. Chem. B. 106 (2002) 6566–6580. doi:10.1021/jp013841g.

[19] L. Milazzo, L. Tognaccini, B.D. Howes, G. Smulevich, Probing the non-native states of Cytochrome c with resonance Raman spectroscopy: A tool for investigating the structure–function relationship, J. Raman Spectrosc. 49 (2018) 1041–1055. doi:10.1002/jrs.5315.

[20] C.J. Nelson, B.E. Bowler, pH Dependence of Formation of a Partially Unfolded State of a Lys 73 → His Variant of Iso-1-cytochrome c: Implications for the Alkaline

Conformational Transition of Cytochrome c, Biochemistry. 39 (2000) 13584–13594. doi:10.1021/bi0017778.
[21] L. Hoang, H. Maity, M.M.G. Krishna, Y. Lin, S.W. Englander, Folding Units Govern the Cytochrome c Alkaline Transition, J. Mol. Biol. 331 (2003) 37–43. doi:10.1016/S0022-2836(03)00698-3.
[22] D. Alvarez-Paggi, D.F. Martín, P.M. Debiase, P. Hildebrandt, M.A. Martí, D.H. Murgida, Molecular basis of coupled protein and electron transfer dynamics of cytochrome c in biomimetic complexes, J. Am. Chem. Soc. 132 (2010) 5769–5778. doi:10.1021/ja910707r.
[23] M.M. Elmer-Dixon, B.E. Bowler, Electrostatic Constituents of the Interaction of Cardiolipin with Site A of Cytochrome c, Biochemistry. 57 (2018) 5683–5695. doi:10.1021/acs.biochem.8b00704.
[24] B. De, D.A. Paggi, F. Doctorovich, P. Hildebrandt, D.A. Estrin, D.H. Murgida, M.A. Marti, Molecular basis for the electric field modulation of cytochrome c structure and function, J. Am. Chem. Soc. 131 (2009) 16248–16256. doi:10.1021/ja906726n.
[25] D. Alvarez-Paggi, M.A. Castro, V. Tórtora, L. Castro, R. Radi, D.H. Murgida, Electrostatically driven second-sphere ligand switch between high and low reorganization energy forms of native cytochrome c, J. Am. Chem. Soc. 135 (2013) 4389–4397. doi:10.1021/ja311786b.
[26] D.A. Capdevila, R. Oviedo, F. Tomasina, V. Tortora, V. Demicheli, R. Radi, D.H. Murgida, Active Site Structure and Peroxidase Activity of Oxidatively Modified Cytochrome c Species in Complexes with Cardiolipin, Biochemistry. 54 (2015) 7491–7504. doi:10.1021/acs.biochem.5b00922.
[27] L.A. Abriata, A. Cassina, V. Tórtora, M. Marín, J.M. Souza, L. Castro, A.J. Vila, R. Radi, Nitration of Solvent-exposed Tyrosine 74 on Cytochrome c Triggers Heme Iron-Methionine 80 Bond Disruption. Nuclear Magnetic Resonance and Optical Spectroscopy Studies, J. Biol. Chem. 284 (2009) 17–26. doi:10.1074/jbc.M807203200.
[28] D.A. Capdevila, D. Álvarez-Paggi, M.A. Castro, V. Tórtora, V. Demicheli, D.A. Estrín, R. Radi, D.H. Murgida, Coupling of tyrosine deprotonation and axial ligand exchange in nitrocytochrome c, Chem. Commun. 50 (2014) 2592–2594. doi:10.1039/C3CC47207H.
[29] H. Theorell, Å. Åkesson, Studies on Cytochrome c. III. Titration Curves, J. Am. Chem. Soc. 63 (1941) 1818–1820. doi:10.1021/ja01852a007.
[30] P.M. Gadsby, J. Peterson, N. Foote, C. Greenwood, A.J. Thomson, Identification of the ligand-exchange process in the alkaline transition of horse heart cytochrome c, Biochem. J. 246 (1987) 43–54. doi:10.1042/bj2460043.
[31] F.I. Rosell, J.C. Ferrer, A.G. Mauk, Proton-Linked Protein Conformational Switching: Definition of the Alkaline Conformational Transition of Yeast Iso-1-ferricytochrome c, J. Am. Chem. Soc. 120 (1998) 11234–11245. doi:10.1021/ja971756+.
[32] S. Döpner, P. Hildebrandt, F.I. Rosell, A.G. Mauk, Alkaline Conformational Transitions of Ferricytochrome c Studied by Resonance Raman Spectroscopy, J. Am. Chem. Soc. 120 (1998) 11246–11255. doi:10.1021/ja9717572.
[33] J.F. Amacher, F. Zhong, G.P. Lisi, M.Q. Zhu, S.L. Alden, K.R. Hoke, D.R. Madden, E.V. Pletneva, A Compact Structure of Cytochrome c Trapped in a Lysine-Ligated State: Loop Refolding and Functional Implications of a Conformational Switch, J. Am. Chem. Soc. 137 (2015) 8435–8449. doi:10.1021/jacs.5b01493.

[34] M. Assfalg, I. Bertini, A. Dolfi, P. Turano, A.G. Mauk, F.I. Rosell, H.B. Gray, Structural Model for an Alkaline Form of Ferricytochrome c, J. Am. Chem. Soc. 125 (2003) 2913–2922. doi:10.1021/ja027180s.

[35] D. Alvarez-Paggi, L. Hannibal, M.A. Castro, S. Oviedo-Rouco, V. Demicheli, V. Tórtora, F. Tomasina, R. Radi, D.H. Murgida, Multifunctional Cytochrome c: Learning New Tricks from an Old Dog, Chem. Rev. 117 (2017) 13382–13460. doi:10.1021/acs.chemrev.7b00257.

[36] T.M. Josephs, M.D. Liptak, G. Hughes, A. Lo, R.M. Smith, S.M. Wilbanks, K.L. Bren, E.C. Ledgerwood, Conformational change and human cytochrome c function: mutation of residue 41 modulates caspase activation and destabilizes Met-80 coordination, JBIC J. Biol. Inorg. Chem. 18 (2013) 289–297. doi:10.1007/s00775-012-0973-1.

[37] M. Lek, K.J. Karczewski, E.V. Minikel, K.E. Samocha, E. Banks, T. Fennell, A.H. O'Donnell-Luria, J.S. Ware, A.J. Hill, B.B. Cummings, T. Tukiainen, D.P. Birnbaum, J.A. Kosmicki, L.E. Duncan, K. Estrada, F. Zhao, J. Zou, E. Pierce-Hoffman, J. Berghout, D.N. Cooper, N. Deflaux, M. DePristo, R. Do, J. Flannick, M. Fromer, L. Gauthier, J. Goldstein, N. Gupta, D. Howrigan, A. Kiezun, M.I. Kurki, A.L. Moonshine, P. Natarajan, L. Orozco, G.M. Peloso, R. Poplin, M.A. Rivas, V. Ruano-Rubio, S.A. Rose, D.M. Ruderfer, K. Shakir, P.D. Stenson, C. Stevens, B.P. Thomas, G. Tiao, M.T. Tusie-Luna, B. Weisburd, H.-H. Won, D. Yu, D.M. Altshuler, D. Ardissino, M. Boehnke, J. Danesh, S. Donnelly, R. Elosua, J.C. Florez, S.B. Gabriel, G. Getz, S.J. Glatt, C.M. Hultman, S. Kathiresan, M. Laakso, S. McCarroll, M.I. McCarthy, D. McGovern, R. McPherson, B.M. Neale, A. Palotie, S.M. Purcell, D. Saleheen, J.M. Scharf, P. Sklar, P.F. Sullivan, J. Tuomilehto, M.T. Tsuang, H.C. Watkins, J.G. Wilson, M.J. Daly, D.G. MacArthur, Exome Aggregation Consortium, Analysis of protein-coding genetic variation in 60,706 humans, Nature. 536 (2016) 285–291. doi:10.1038/nature19057.

[38] R.M. Kluck, L.M. Ellerby, H.M. Ellerby, S. Naiem, M.P. Yaffe, E. Margoliash, D. Bredesen, A.G. Mauk, F. Sherman, D.D. Newmeyer, Determinants of Cytochrome c Pro-apoptotic Activity. The Role of Lysine 72 Trimethylation, J. Biol. Chem. 275 (2000) 16127–16133. doi:10.1074/jbc.275.21.16127.

[39] S.C. Kim, R. Sprung, Y. Chen, Y. Xu, H. Ball, J. Pei, T. Cheng, Y. Kho, H. Xiao, L. Xiao, N.V. Grishin, M. White, X.-J. Yang, Y. Zhao, Substrate and Functional Diversity of Lysine Acetylation Revealed by a Proteomics Survey, Mol. Cell. 23 (2006) 607–618. doi:10.1016/j.molcel.2006.06.026.

[40] L.A. Davis, A. Schejter, G.P. Hess, Alkaline Isomerization of Oxidized Cytochrome c. Equilibrium and Kinetic Measurements, J. Biol. Chem. 249 (1974) 2624–2632.

[41] J.D. Cortese, A.L. Voglino, C.R. Hackenbrock, Persistence of cytochrome c binding to membranes at physiological mitochondrial intermembrane space ionic strength, Biochim. Biophys. Acta BBA - Bioenerg. 1228 (1995) 216–228. doi:10.1016/0005-2728(94)00178-8.

[42] H. Kobayashi, S. Nagao, S. Hirota, Characterization of the Cytochrome c Membrane-Binding Site Using Cardiolipin-Containing Bicelles with NMR, Angew. Chem. Int. Ed. 55 (2016) 14019–14022. doi:10.1002/anie.201607419.

[43] D.H. Murgida, P. Hildebrandt, Electron-transfer processes of cytochrome c at interfaces. New insights by surface-enhanced resonance Raman spectroscopy, Acc. Chem. Res. 37 (2004) 854–861. doi:10.1021/ar0400443.

[44] D.H. Murgida, P. Hildebrandt, Redox and redox-coupled processes of heme proteins and enzymes at electrochemical interfaces, Phys. Chem. Chem. Phys. 7 (2005) 3773–3784. doi:10.1039/b507989f.
[45] D.H. Murgida, P. Hildebrandt, Disentangling interfacial redox processes of proteins by SERR spectroscopy, Chem. Soc. Rev. 37 (2008) 937–945. doi:10.1039/b705976k.
[46] F. Sinibaldi, L. Milazzo, B.D. Howes, M.C. Piro, L. Fiorucci, F. Polticelli, P. Ascenzi, M. Coletta, G. Smulevich, R. Santucci, The key role played by charge in the interaction of cytochrome c with cardiolipin, JBIC J. Biol. Inorg. Chem. 22 (2017) 19–29. doi:10.1007/s00775-016-1404-5.
[47] D. Alvarez-Paggi, W. Meister, U. Kuhlmann, I. Weidinger, K. Tenger, L. Zimányi, G. Rákhely, P. Hildebrandt, D.H. Murgida, Disentangling electron tunneling and protein dynamics of cytochrome c through a rationally designed surface mutation, J. Phys. Chem. B. 117 (2013) 6061–6068. doi:10.1021/jp400832m.
[48] M.M. Cherney, C.C. Junior, B.B. Bergquist, B.E. Bowler, Dynamics of the His79-Heme Alkaline Transition of Yeast Iso-1-cytochrome c Probed by Conformationally Gated Electron Transfer with Co(II)bis(terpyridine), J. Am. Chem. Soc. 135 (2013) 12772–12782. doi:10.1021/ja405725f.
[49] S. Bandi, B.E. Bowler, A cytochrome C electron transfer switch modulated by heme ligation and isomerization of a peptidyl-prolyl bond, Pept. Sci. 100 (2013) 114–124. doi:10.1002/bip.22164.
[50] S. Döpner, P. Hildebrandt, A. Grant Mauk, H. Lenk, W. Stempfle, Analysis of vibrational spectra of multicomponent systems. Application to pH-dependent resonance Raman spectra of ferricytochrome c, Spectrochim. Acta. A. Mol. Biomol. Spectrosc. 52 (1996) 573–584. doi:10.1016/0584-8539(95)01647-3.
[51] AMBER 2016, University of California, San Francisco, 2016.
[52] H.J.C. Berendsen, J.P.M. Postma, W.F. van Gunsteren, A. DiNola, J.R. Haak, Molecular dynamics with coupling to an external bath, J. Chem. Phys. 81 (1984) 3684–3690. doi:10.1063/1.448118.
[53] J.-P. Ryckaert, G. Ciccotti, H.J.C. Berendsen, Numerical integration of the cartesian equations of motion of a system with constraints: molecular dynamics of n-alkanes, J. Comput. Phys. 23 (1977) 327–341. doi:10.1016/0021-9991(77)90098-5.
[54] D.M. Moreno, M.A. Martí, P.M. De Biase, D.A. Estrin, V. Demicheli, R. Radi, L. Boechi, Exploring the molecular basis of human manganese superoxide dismutase inactivation mediated by tyrosine 34 nitration, Arch. Biochem. Biophys. 507 (2011) 304–309. doi:10.1016/j.abb.2010.12.011.
[55] J. Mongan, D.A. Case, J.A. McCammon, Constant pH molecular dynamics in generalized Born implicit solvent, J. Comput. Chem. 25 (2004) 2038–2048. doi:10.1002/jcc.20139.
[56] N. Metropolis, A.W. Rosenbluth, M.N. Rosenbluth, A.H. Teller, E. Teller, Equation of State Calculations by Fast Computing Machines, J. Chem. Phys. 21 (1953) 1087–1092. doi:10.1063/1.1699114.
[57] D.H. Murgida, P. Hildebrandt, Heterogeneous electron transfer of cytochrome c on coated silver electrodes. Electric field effects on structure and redox potential, J. Phys. Chem. B. 105 (2001) 1578–1586.
[58] J. Petrović, R.A. Clark, H. Yue, D.H. Waldeck, E.F. Bowden, Impact of Surface Immobilization and Solution Ionic Strength on the Formal Potential of Immobilized Cytochrome c, Langmuir. 21 (2005) 6308–6316. doi:10.1021/la0500373.

[59] G. Battistuzzi, M. Borsari, L. Loschi, A. Martinelli, M. Sola, Thermodynamics of the Alkaline Transition of Cytochrome c, Biochemistry. 38 (1999) 7900–7907. doi:10.1021/bi983060e.
[60] A. Kranich, H.K. Ly, P. Hildebrandt, D.H. Murgida, Direct observation of the gating step in protein electron transfer: Electric-field-controlled protein dynamics, J. Am. Chem. Soc. 130 (2008) 9844–9848. doi:10.1021/ja8016895.
[61] D.A. Paggi, D.F. Martín, A. Kranich, P. Hildebrandt, M.A. Martí, D.H. Murgida, Computer simulation and SERR detection of cytochrome c dynamics at SAM-coated electrodes, Electrochimica Acta. 54 (2009) 4963–4970. doi:10.1016/j.electacta.2009.02.050.
[62] G. Battistuzzi, M. Borsari, F. De Rienzo, G. Di Rocco, A. Ranieri, M. Sola, Free Energy of Transition for the Individual Alkaline Conformers of Yeast Iso-1-cytochrome c, Biochemistry. 46 (2007) 1694–1702. doi:10.1021/bi061961e.
[63] R.T. Hartshorn, G.R. Moore, A denaturation-induced proton-uptake study of horse ferricytochrome c., Biochem. J. 258 (1989) 595–598.
[64] G.G. Silkstone, C.E. Cooper, D. Svistunenko, M.T. Wilson, EPR and Optical Spectroscopic Studies of Met80X Mutants of Yeast Ferricytochrome c. Models for Intermediates in the Alkaline Transition, J. Am. Chem. Soc. 127 (2005) 92–99. doi:10.1021/ja045719b.
[65] F.I. Rosell, T.R. Harris, D.P. Hildebrand, S. Döpner, P. Hildebrandt, A.G. Mauk, Characterization of an Alkaline Transition Intermediate Stabilized in the Phe82Trp Variant of Yeast iso-1-Cytochrome c, Biochemistry. 39 (2000) 9047–9054. doi:10.1021/bi001095k.
[66] O.M. Deacon, D.A. Svistunenko, G.R. Moore, M.T. Wilson, J.A.R. Worrall, Naturally Occurring Disease-Related Mutations in the 40–57 Ω-Loop of Human Cytochrome c Control Triggering of the Alkaline Isomerization, Biochemistry. 57 (2018) 4276–4288. doi:10.1021/acs.biochem.8b00520.
[67] S. Zaidi, M.I. Hassan, A. Islam, F. Ahmad, The role of key residues in structure, function, and stability of cytochrome c, Cell. Mol. Life Sci. 71 (2014) 229–255. doi:10.1007/s00018-013-1341-1.
[68] J. Santo-Domingo, N. Demaurex, The renaissance of mitochondrial pH, J. Gen. Physiol. 139 (2012) 415–423. doi:10.1085/jgp.201110767.

GRAPHICAL ABSTRACT